Design of High Frequency Ultrasonic Transducers with Flexure Decoupling Flanges for Thermosonic Bonding

***Abstract*—This paper presents the design of high frequency ultrasonic transducers for microelectronic thermosonic bonding. The transducers are actuated by piezoelectric ceramics and decoupled with their connecting parts through novel flexure decoupling flanges. Firstly, the initial geometric dimensions of the transducers were calculated using electromechanical equivalent method, and then the dynamic optimization design were carried out based on 3D finite element method (FEM) using ANSYS software, and the geometric dimensions of the transducer were finally determined. Flexure decoupling flanges were presented, and the decoupling principle of the flanges was explained through compliance modeling using compliance matrix method and FEM. After that the dynamic characteristic of the transducers were analyzed through finite element analysis (FEA) using ANSYS software. The vibration frequencies and modes of the piezoelectric converter, concentrators and transducers were obtained through modal analysis, respectively and the displacement nodes were determined. The longitudinal ultrasonic energy transmission was presented and the decoupling effects of the flexure flanges were compared. Finally, the transducers were manufactured and experimental tests were conducted to examine the transducer characteristics using an impedance analyzer. The experimental results match well with the FEA. The results show that the longitudinal vibration frequencies of the transducers with ring, prismatic beam and circular notched hinge based flanges are 126.6 kHz, 125.8 kHz and 125.52 kHz, respectively. The decoupling flange with circular notched hinges shows the best decoupling effect among the three types of flanges. There are no other vibration modes parasitizing closely to the longitudinal vibration mode.**

***Index Terms*—Ultrasonic transducers, Flexure decoupling, Optimization design, Dynamic characteristics, Impedance test**

I. Introduction

RECENTLY, the trend towards miniaturizing products such as MEMS and NEMS devices has stimulated extensive research on automated micro/nano positioning, manufacturing and packaging techniques [1]-[4]. As important components of microelectronic packaging techniques, thermosonic wire bonding and flip chip bonding, can achieve electrical interconnections between microelectronic devices and their substrates [5]. During thermosonic bonding, ultrasonic energy, heat and pressure are applied simultaneously. Fig.1 shows a typical thermosonic wire bonding process, where ultrasonic transducer plays an important role in terms of converting electronic energy into ultrasonic energy, and then transmitting the energy to the bonding interfaces, and its characteristics have significant influence on the bonding speed and quality [6]. As a result, it is necessary to develop novel ultrasonic transducers with high performance to satisfy the stringent performance requirements of modern microelectronic thermosonic bonding.

Many interesting works have been reported on the design of ultrasonic transducers used for thermosonic bonding [7], among which the transducer actuation principles, mechanical structure, design and analysis method are commonly emphasized during the design process.

Giant magnetostrictive material has unique characteristics of high power density, great output force and fast response, and thus it can be used as the actuator of ultrasonic transducers [8], [9]. However, due to the inherent hysteresis of the giant magnetostrictive material, it is difficult to precisely control this kind of actuator and thus its further applications are limited. Because of the advantages of high force output to weight ratio, fast response, high electromechanical coupling factor and piezoelectric constant, piezoelectric ceramics have been widely used in many fields [10], [11], including the ultrasonic applications [12]-[14].

The mechanical structures of transducers have an important effect on their characteristics, and they can affect the ultrasonic generation and transmission. In the literature, different transducer mechanisms have been proposed. Narasimalu and Balakrishnan presented a novel transducer with an isosceles triangle cross-section concentrator [15]. Sakakura designed a hollow structure transducer to reduce the external environmental influence, and thus the ultrasonic energy efficiency was improved [16]. In addition, serial [17] and parallel [18] structure transducers were developed to improve the vibration amplitudes and frequencies. Form above reported transducers, it is known that the sandwich structure have been being considered as the basic element of the transducers for thermosonic bonding.

The design and characteristic analysis of ultrasonic transducers have been received considerable attention from

researchers. In the literature, some analytical methods include the wave and vibration theory and electromechanical equivalent method were used to model and design transducers, however, the calculations were not so accurate because there are usually some assumptions [19]-[22]. The transducers designed using these analytical methods usually need to be repeatedly modified through experiments to satisfy the performance requirement. To facilitate the design process, finite element method (FEM) has been adopted [23]. Or et al. analyzed the dynamics of a transducer using finite element software without considering the piezoelectric effect of the actuators [24], [25]. An approach to design ultrasonic transducers for thermosonic bonding was presented by Parrini based on modularity and iterations principles, however, how to obtain the initial geometric dimensions of transducers were not effectively presented. In addition, the design was based on the repeated FEM modeling and calculations, and thus the design efficiency is low [26].

For fine-pitch and high-speed thermosonic bonding, higher frequency transducers are required because it can reduce bonding temperature and shorten bonding time, however, because the high frequency transducer for thermosonic bonding usually works at their frequency multiplication, there are some other undesirable vibrations parasitizing closely to the longitudinal vibration mode, making it difficult to control [27], [28]. Another particular issue is the transducer clamping. The ultrasonic energy conversion efficiency is sensitive to the clamping style, especially for high frequency transducers for thermosonic bonding [23], [26]. To minimize the ultrasonic energy loss into the connecting part, the clamping point should be placed in the longitudinal and radial displacement nodes of the ultrasonic field. However, the positions of the displacement nodes are not always calculated so accurately. Most of the presently used transducers for thermosonic bonding adopt rigid connection flanges, and thus the ultrasonic conversion efficiency is not high because the displacement nodes are not located in an ideal plane and also the flanges always have a certain thickness [24]-[26].

This paper presents the design of high frequency sandwich piezoelectric transducers for thermosonic bonding and the design process consists of three phases: initial geometric dimensions calculation using electromechanical equivalent theory, dynamic optimization design and analysis based on FEM using ANSYS software and experimental impedance tests. In addition, flexible decoupling flanges are presented to improve the ultrasonic energy conversion efficiency.

The rest of the paper is organized as follows: Section II introduces the transducer design without flanges, and the flexure decoupling flanges are presented in section III, Then, the dynamic characteristics of the transducer are analyzed in section IV. After that experimental impedance tests are carried out in Section V to examine the design method and the performance of the developed transducers. Finally, Section VI concludes this paper.

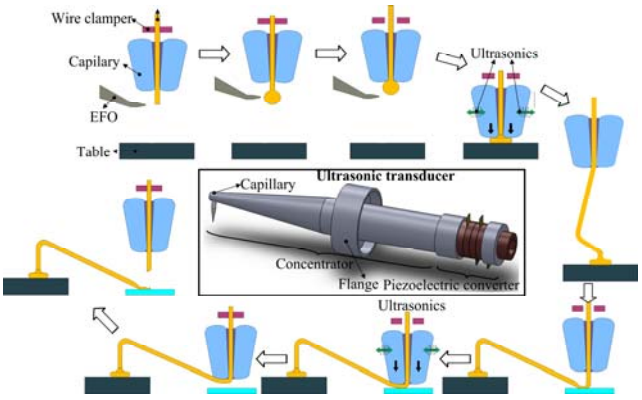

Fig. 1. Theromosonic wire bonding process and the ultrasonic transducer.

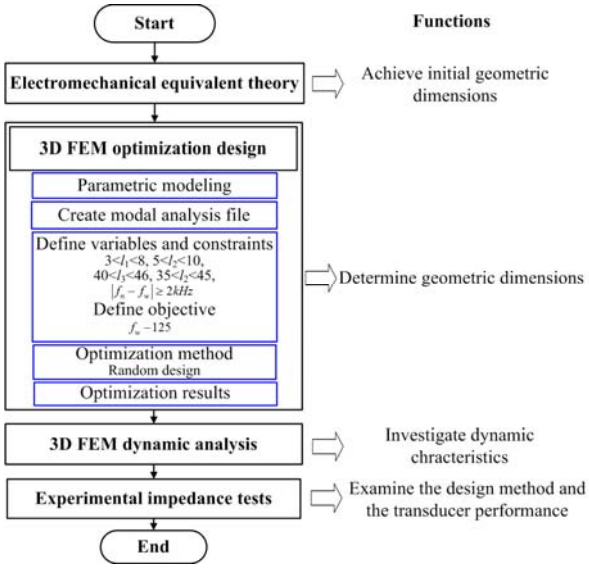

Fig. 2. The design process

II. TRANSDUCER DESIGN WITHOUT FLANGES

The design process is illustrated in Fig.2. The design begins with calculation the initial geometric dimensions of the transducers using the electromechanical equivalent theory. Then the transducers are dynamically optimized and analyzed based on 3D FEM using ANSYS software, and the geometric dimensions are finally determined. At last, experimental impedance tests are carried out to examine the design method and the performance of the developed transducers.

A. Initial geometric dimension calculation based on electromechanical equivalent method

Electromechanical equivalent method is adopted to calculate the initial dimensions of the transducers based on the similarity between mechanical vibration and electrical resonance. The electromechanical equivalent circuitry of a sandwich ultrasonic transducer is shown in Fig.3, where Z is defined as the impedance related to the size, material and resonance frequency of the transducer components, Z_{1p} and Z_{2p} are the equivalent impedances of piezoelectric ceramic stack, Z_{11}, Z_{12} and Z_{13} are the equivalent impedances of the back slab, Z_{21}, Z_{22} and Z_{23} are

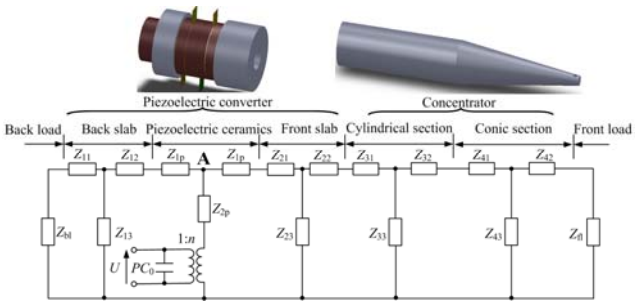

Fig. 3. Electromechanical equivalent circuitry of an ultrasonic transducer.

the equivalent impedances of the front slab, Z_{31}, Z_{32} and Z_{33} are the equivalent impedances of the concentrator cylindrical section, Z_{41}, Z_{42} and Z_{43} are the equivalent impedances of the concentrator conic section, Z_{fl} and Z_{bl} are the radiant impedances of the transducer in the front and back directions, p is the number of the ceramics, C_0 is the one dimension cut-off capacitance of the piezoelectric ceramic, n is the electronmechanical conversion coefficient of the ceramic, and U is the voltage applied to the transducer.

For the piezoelectric ceramic stack, the impedances can be calculated by [29]

$$Z_{1p} = j\rho_{pzt} c_e S_{pzt} \tan(pk_{pzt} l_{pzt}/2) \tag{1}$$

$$Z_{2p} = \frac{\rho_{pzt} c_e S_{pzt}}{j \sin pk_e l_{pzt}} \tag{2}$$

$$k_{pzt} = \frac{\omega_{pzt}}{c_e} \tag{3}$$

where ρ_{pzt} is the ceramic density, c_e is the sound speed of ceramic stack longitudinal vibration, S_{pzt} is the cross-section area of the ceramics, ω_{pzt} is the vibration frequency, n is the electro-mechanical conversion coefficient and l_{pzt} is the thickness of a piece of the ceramic.

For the back and front slabs, and the concentrator cylindrical section, the impedances can be calculated by [29]

$$Z_{i1} = \frac{\rho_i c_i K_i S_i}{jk_i} \cot(K_i l_i) - \frac{\rho_i c_i K_i S_i}{jk_i \sin(K_i l_i)} \qquad i = 1,2,3 \tag{4}$$

$$Z_{i2} = Z_{i1} = \frac{\rho_i c_i K_i S_i}{jk_i} \cot(K_i l_i) - \frac{\rho_i c_i K_i S_i}{jk_i \sin(K_i l_i)} \qquad i = 1,2,3 \tag{5}$$

$$Z_{i3} = \frac{\rho_i c_i K_i S_i}{jk_i \sin(K_i l_i)} \qquad i = 1,2,3 \tag{6}$$

$$k_i = \frac{\omega_i}{c_i} \qquad i = 1,2,3 \tag{7}$$

$$K_i^2 = k_i^2 - \frac{1}{\sqrt{S_i}} \frac{\partial^2 \left(\sqrt{S_i}\right)}{\partial x^2} \qquad i = 1,2,3 \tag{8}$$

where ρ_1, ρ_2 and ρ_3 are the density of the back slab, front slab and the concentrator cylindrical section, respectively, c_1, c_2 and c_3 are the longitudinal vibration speed of the back slab, front slab and concentrator cylindrical section, respectively, S_1, S_2 and S_3 are the cross-section areas of the back slab, front slab and concentrator cylindrical section, respectively, ω_1, ω_2 and ω_3 are the vibration frequencies of the back slab, front slab and concentrator cylindrical section, respectively, and l_1, l_2 and l_3 are the thicknesses of the back slab, front slab and concentrator cylindrical section, respectively.

The impedances of the concentrator conic section can be expressed as [29]

$$Z_{41} = -j\frac{\rho_4 c_4 S_{41}}{k_4 l_4}\left(\frac{\sqrt{S_{42}}}{\sqrt{S_{41}}} - 1\right) - j\rho_4 c_4 S_{41} ctg\left(k_4 l_4\right) + j\frac{\rho_4 c_4 \sqrt{S_{41} S_{42}}}{\sin k_4 l_4} \tag{9}$$

$$Z_{42} = -j\frac{\rho_4 c_4 S_{42}}{k_4 l_4}\left(\frac{\sqrt{S_{41}}}{\sqrt{S_{42}}} - 1\right) - j\rho_4 c_4 S_{42} ctg\left(k_4 l_4\right) + j\frac{\rho_4 c_4 \sqrt{S_{41} S_{42}}}{\sin k_4 l_4} \tag{10}$$

$$Z_{43} = \frac{\rho_4 c_4 \sqrt{S_{41} S_{42}}}{\sin k_4 l_4} \tag{11}$$

$$k_4 = \frac{\omega_4}{c_4} \tag{12}$$

where ρ_4, c_4, S_{41}, S_{42}, ω_4 and l_4 are the density, longitudinal vibration speed, the smallest and largest cross-section areas, vibration frequency, and the thickness of the concentrator conic section, respectively.

According to Kirchhoff's law, the total electric impedance of the transducer can be expressed by

$$Z_e = \frac{Z_{C0} n^2 Z_m}{Z_{C0} + n^2 Z_m} = \mathrm{Re}(Z_e) + \mathrm{Im}(Z_e) \tag{13}$$

where $Z_{C0} = \frac{1}{j\omega_{pzt} pC_0}$, $Z_m = Z_{2p} + \frac{Z_{AR} Z_{AL}}{Z_{AR} + Z_{AL}}$, $Z_{AR} = Z_{1p} + Z_1$, $Z_{AL} = Z_{1p} + Z_2$, $Z_1 = Z_{12} + \frac{Z_{13}\left(Z_{11} + Z_{bl}\right)}{Z_{13} + \left(Z_{11} + Z_{bl}\right)}$, $Z_2 = Z_{21} + \frac{Z_{22}\left(Z_{23} + Z_3\right)}{Z_{22} + \left(Z_{23} + Z_3\right)}$, $Z_3 = Z_{31} + \frac{Z_{32}\left(Z_{33} + Z_4\right)}{Z_{32} + \left(Z_{33} + Z_4\right)}$ and $Z_4 = Z_{41} + \frac{Z_{42}\left(Z_{43} + Z_{fl}\right)}{Z_{42} + \left(Z_{43} + Z_{fl}\right)}$.

The resonance frequency equation of the transducer can be written as follows:

$$Z_{C0} n^2 Z_m = 0 \tag{14}$$

Thus the initial geometrical dimensions of the transducer can be calculated based on eqs.(13) and (14). The working mode vibration frequency is designed as 125 kHz and the results are summarized in Table 1.

TABLE I
INITIAL GEOMETRIC DIMENSIONS OF THE TRANSDUCERS

Parameters	l_{pzt}	l_1	l_2	l_3	l_4
Value(mm)	2.3	5.5	7.5	43	40

B. 3D FEM optimization

The geometric dimensions of the transducer are finally determined through 3D FEM optimization using ASNSYS software. As shown in Fig.2, the 3D parametric FEM model is first established using ANSYS APDL based on the initial geometric dimensions obtained using electromechanical equivalent method. The variables, constraints and objective for the optimization are defined and shown in Fig.2, where f_m is the designed working mode frequency, and f_n is the frequency of the adjacent vibration mode of the working mode. To reduce vibration mode density and avoid mode coupling effect, we keep $|f_n - f_m| \geq 2$ kHz. Random design method is adopted for the optimization and the geometric dimensions of the transducers are determined and shown in Table II, where d_I is the inner diameter of the front slab, ceramics and back slab, and d_{pO}, d_{1O} and d_{2O} are the outer diameters of the ceramics, front and back slabs, respectively.

TABLE II
FINAL GEOMETRIC DIMENSIONS OF THE TRANSDUCERS

Parameters	l_{pzt}	l_1	l_2	l_3	l_4	d_I	d_{pO}	d_{1O}	d_{2O}
Value(mm)	2.3	5.2	6.8	41.6	39.2	5	13	15	15

III. FLEXURE DECOUPLING FLANGES

To improve the ultrasonic conversion efficiency, flexure hinge based flanges are adopted as the decoupling mechanism between the transducers and their connecting parts. The decoupling is realized through the flexure deformation of the flexure hinges. Three types of decoupling flanges, namely ring, plasmatic beam, and circular notched hinges based flanges, are presented and shown in Fig.4.

Because the decoupling is based on the flexure deformation of the hinge based mechanism, the longitudinal stiffnesses of the decoupling flanges are investigated. Considering the ring can be divided into several beams, the stiffness of ring hinge based flange is larger than the prismatic beam based flange. Stiffness comparison is carried out to the prismatic beam and circular notched hinge based flanges and compliance matrix method is adopted for the modeling.

For the hinges shown in Fig.5, eq.(15) shows their tip deformations when forces and moments are applied on them.

$$\boldsymbol{X} = \boldsymbol{CF} \tag{15}$$

where $\boldsymbol{X}$ is the deformations, $\boldsymbol{F}$ is the forces and moments, $\boldsymbol{C}$ is the compliance matrix, and the stiffness matrix $\boldsymbol{K}=1/\boldsymbol{C}$.

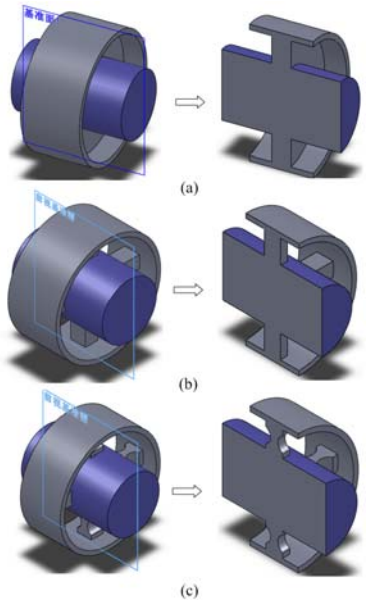

Fig. 4. Three types of decoupling flanges: (a) ring, (b) prismatic beam (3) circular notched hinge based flanges.

Eq.(15) can be rewritten as

$$\begin{pmatrix} \delta_x \\ \delta_y \\ \delta_z \\ \theta_x \\ \theta_y \\ \theta_z \end{pmatrix} = \begin{pmatrix} C_1 & 0 & 0 & 0 & C_3 & 0 \\ 0 & C_2 & 0 & -C_4 & 0 & 0 \\ 0 & 0 & C_5 & 0 & 0 & 0 \\ 0 & -C_4 & 0 & C_6 & 0 & 0 \\ C_3 & 0 & 0 & 0 & C_7 & 0 \\ 0 & 0 & 0 & 0 & 0 & C_8 \end{pmatrix} \begin{pmatrix} F_x \\ F_y \\ F_z \\ M_x \\ M_y \\ M_z \end{pmatrix} \tag{16}$$

For the decoupling flanges shown in Fig.6, the compliance can be represented by

$$\boldsymbol{C}_{ABCD} = \begin{pmatrix} \boldsymbol{C}_A & 0 & 0 & 0 \\ 0 & \boldsymbol{C}_B & 0 & 0 \\ 0 & 0 & \boldsymbol{C}_C & 0 \\ 0 & 0 & 0 & \boldsymbol{C}_D \end{pmatrix} \tag{17}$$

where $\boldsymbol{C}_A$, $\boldsymbol{C}_B$, $\boldsymbol{C}_C$ and $\boldsymbol{C}_D$ are the compliance matrices at points A, B, C and D, respectively.

For the prismatic beam based flange, the compliance C_1^{beam} in the compliance matrix $\boldsymbol{C}_A^{Beam}$ can be calculated as

$$C_1^{beam} = \frac{4l^3}{Ea^3b} = \frac{4\left(l_{C1} + 2r + l_{C2}\right)^3}{Ea^3b} \tag{18}$$

where E is the modulus of elasticity.

For the circular notched hinge based flange, the compliance $\boldsymbol{C}_A^{Circular}$ can be calculated as

$$\begin{aligned} C_A^{circular} = {} & \boldsymbol{C}_{prism}(a,b,l_{C1}) + \boldsymbol{P}(0,0,l_{C1})\boldsymbol{C}_{circular}(r,t,b)\boldsymbol{P}^{\boldsymbol{T}}(0,0,l_{C1}) \\ & + \boldsymbol{P}(0,0,l_{C1}+2r)\boldsymbol{C}_{prism}(a,b,l_{C2})\boldsymbol{P}^{T}(0,0,l_{C1}+2r) \end{aligned}$$

(19)

where $\boldsymbol{P}(0,0,l_{C1})$ and $\boldsymbol{P}(0,0,l_{C1}+2r)$ are the translational transformation matrices, and can be expressed by

$$\boldsymbol{P}(0,0,l_{C1})=\begin{pmatrix}1&0&0&0&l_{C1}&0\\0&1&0&-l_{C1}&0&0\\0&0&1&0&0&0\\0&0&0&1&0&0\\0&0&0&0&1&0\\0&0&0&0&0&1\end{pmatrix} \tag{20}$$

$$\boldsymbol{P}(0,0,l_{C1}+2r)=\begin{pmatrix}1&0&0&0&l_{C1}+2r&0\\0&1&0&-(l_{C1}+2r)&0&0\\0&0&1&0&0&0\\0&0&0&1&0&0\\0&0&0&0&1&0\\0&0&0&0&0&1\end{pmatrix} \tag{21}$$

The compliance $C_1^{cirular}$ in the compliance matrix $\boldsymbol{C}_A^{circular}$ can be achieved as

$$C_1^{Circular}=\frac{4l_{C1}^{\ 3}}{Ea^3b}+\frac{9\pi r^{2.5}}{2Ebt^{2.5}}+\frac{3\pi r^{1.5}}{2Ebt^{1.5}}+l_{C1}\frac{9\pi r^{1.5}}{Ebt^{2.5}}+ l_{C1}^{\ 2}\frac{9\pi r^{0.5}}{2Ebt^{2.5}}+\frac{4l_{C2}^{\ 3}}{Ea^3b}+(l_{C1}+2r)\frac{12l_{C2}^{\ 2}}{Ea^3b}+(l_{C1}+2r)^2\frac{12l_{C2}}{Ea^3b} \tag{22}$$

Thus

$$C_1^{Circular}-C_1^{beam}=C_1^{Circular}-\frac{4(l_{C1}+2r+l_{C2})^3}{Ea^3b}>0 \tag{23}$$

From eq.(23), it is known that the stiffness of prismatic beam based flange is larger than that of the circular notched hinge based flange when they have the same thickness, width and length. That is to say, the circular notched hinge based flange has better decoupling effect compared with the ring and prismatic beam based flanges.

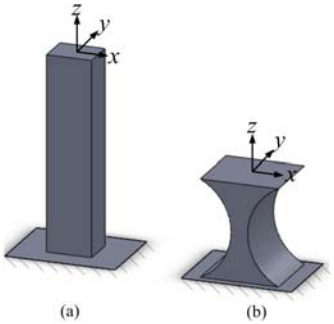

Fig. 5. General hinges: (a) prismatic beam, and (b) circular notched hinge.

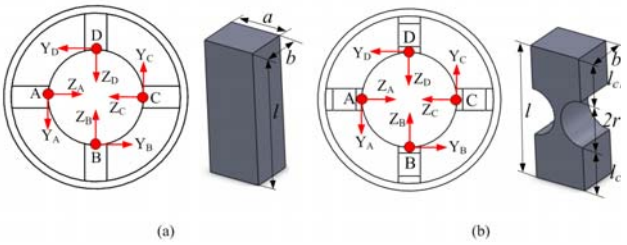

Fig. 6. Chain of the decoupling flanges: (a) prismatic beam, and (b) circular notched hinge based flanges.

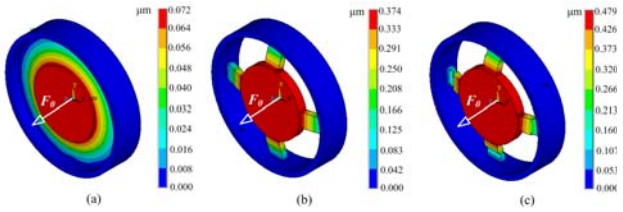

Fig. 7. FEA results for the decoupling flange stiffnesses.

FEA was performed to investigate the stiffnesses of the flanges and the results are shown in Fig.7. When applied the same force to the flanges, the circular notched hinges based flange has the largest deformation, then the prismatic beam and the smallest is the ring based flange. The result matches well with the analytical analysis.

The dimensions of the flexure flanges are shown as follows: For the prismatic beam based flange, $a=4.5\text{mm}$, $b=1.5\text{mm}$ and $l=6\text{mm}$. For the circular notched hinges based flange, $a=4.5\text{mm}$, $b=1.5\text{mm}$, $l=6\text{mm}$, $l_{c1}=2.5\text{mm}$, $l_{c2}=2.5\text{mm}$, $r=0.5\text{mm}$ and $t=0.5\text{mm}$.

IV. Dynamic Characteristic Analysis

Dynamic vibration characteristics were analyzed based on FEM using ANSYS software. The 3D FEM models were established, where piezoelectric coupled element solid5 was utilized to simulate the piezoelectric ceramics, and solid92 element was for the other components of the transducer. Zero voltage was applied to the side surfaces of piezoelectric ceramics to simulate the electrical short circuit conditions, and opposite polarization directions were defined to the adjacent ceramics.

A. Piezoelectric converter

Modal analysis was carried out to the piezoelectric converter, and the longitudinal vibration frequency and corresponding vibration modes were figured out. The results show that the piezoelectric converter vibrates in the longitudinal direction at the frequency of 125.2 kHz. The deformations and the ultrasonic energy transmission in the longitudinal direction are plotted in Fig.8. The piezoelectric converter has a length of half a wavelength and the vibration generated by the piezoelectric ceramics is amplified and transmitted to the front flab.

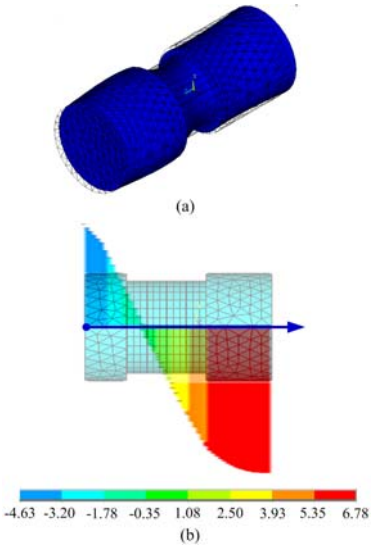

Fig. 8. Vibration characteristics of the piezoelectric converter.

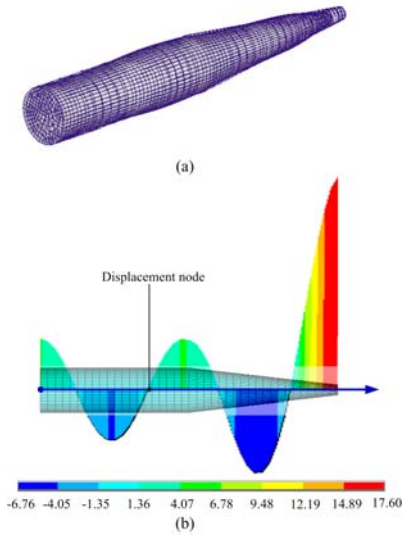

Fig. 9. Vibration characteristics of the concentrator.

B. *Concentrator*

Modal analysis for the concentrator was performed and the results show the longitudinal vibration frequency is 125.6 kHz, and the corresponding deformation and ultrasonic energy transmission in the longitudinal direction are displayed in Fig.9. The vibration is amplified and transmitted to the small tip of the concentrator. In addition, the vibration displacement nodes have been determined.

The decoupling flanges were placed at the vibration displacement nodes, and then the concentrator vibration characteristics with the flanges as well as the decoupling effect of the flanges were investigated. The vibrations of the concentrators and the flanges are depicted in Fig.10. The corresponding vibration frequencies are listed in Table III. It is found that the circular notched hinge based flange can provide larger deformation potential compared with the other two kinds of flanges, and has less influence on the longitudinal vibration frequency, so it exhibits the best decoupling effect among the three types of flanges.

C. *Ultrasonic transducer*

Connecting the piezoelectric converter and concentrators, ultrasonic transducers are obtained. The vibration was analyzed, and the longitudinal vibration frequencies of the transducers are summarized in Table IV. The deformation and ultrasonic energy transmission vector of the transducer with the circular notched hinge based flange at the frequency of 125.58 kHz are shown in Fig.11. The result shows that the ultrasonic vibration was generated by the piezoelectric ceramics, then transmitted to the front slab and amplified by the concentrator. There are no other vibration modes parasitizing closely to the longitudinal vibration mode.

TABLE III
VIBRATION FREQUENCIES OF THE CONCENTRATOR WITH FLANGES

Flange type	Ring	Prismatic beam	Circular notched hinge
Frequency (kHz)	126.16	125.82	125.68

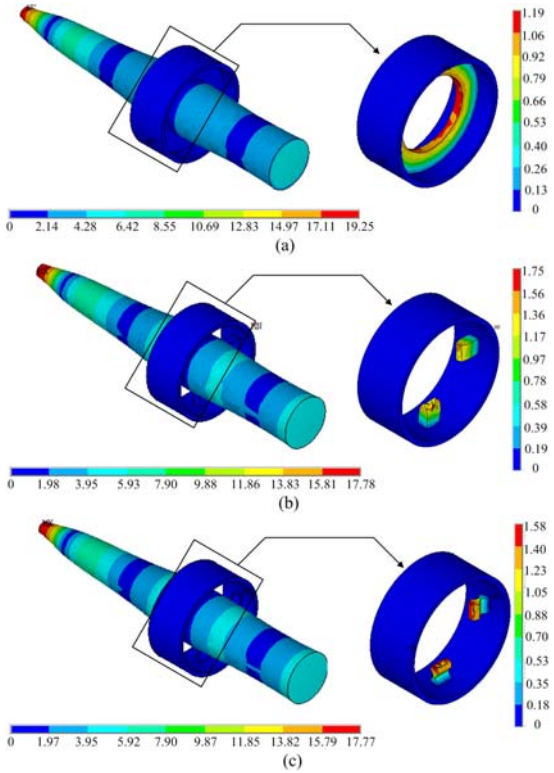

Fig. 10. Vibration characteristics of the concentrators with flanges: (a) Ring, (b) prismatic beam, and (c) circular notched hinge based flanges.

TABLE IV
VIBRATION FREQUENCIES OF THE TRANSDUCERS

Flange type	Ring	Prismatic beam	Circular notched hinge
Frequency (kHz)	126.12	125.70	125.58

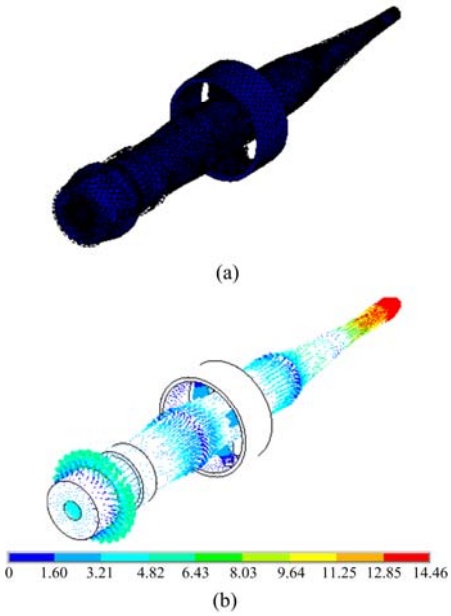

Fig.11. Vibration characteristics of the ultrasonic transducer: (a) deformation, and (b) ultrasonic energy transmission vector.

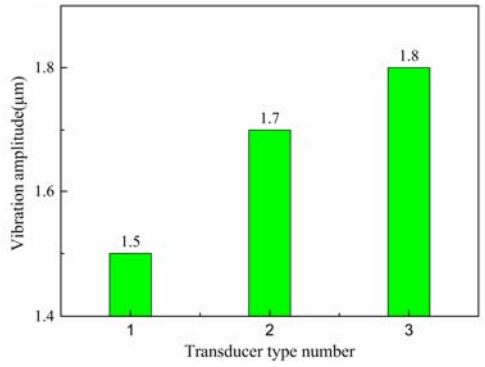

Fig. 12. Vibration amplitude of the transducer tip

Harmonic responses of the transducers were calculated out when the piezoelectric ceramics were applied a voltage of U=10sinωt. The results are shown in Fig.12. The tip displacement amplitude of the transducer with the ring, prismatic beam and circular notched hinge based flanges can reach up to 1.5 μm, 1.7 μm and 1.8 μm, respectively.

V. Experiments

The components of the transducers were manufactured using numerical control (NC) machine tool, and the concentrators with three different decoupling flanges based on the ring, prismatic beam and circular notched flexure hinges are shown in Fig.13.

The transducers have been achieved through assembly of all their components. To investigate the vibration characteristics of the developed transducers, impedance tests were carried out using an impedance analyzer PV70A. The experimental setup for impedance tests are shown in Fig.14. Firstly the transducers were connected electrically with the Impedance Analyzer, and then the voltage exciting signals with the amplitude of 1 V and frequency from 120 to134 kHz were generated by the signal generator, meanwhile the transducer impedance was recorded with the aid of the PV70A and PiezoView software.

The resonant frequencies of the transducers are listed in Table V, and the impedances are shown in Fig.15. The experimental test results are in good agreement with that of the FEA. The three types of flexure hinge based flanges have decoupling effects between the transducers and their connecting parts, among which the decoupling flange with circular notched hinges can provide the largest deformation potential, and it can cause least deviation from the designed frequency. As a result, it shows the best decoupling effect. The ring hinge based flange can generate the smallest deformation, and thus exhibits the worst decoupling effect. It is noted that there are some frequency deviations between FEM simulation and experiments, which is mainly because that simulations are only a rough approximation of the geometry of the vibrating body, and the material property and constraint conditions defined in FEM may be not exactly the same with the experiments. In addition, the modal analysis is usually linear using ANSYS software; however, the real material property parameters and the mechanical structure are not always linear.

Fig. 13. The concentrators with decoupling flanges.

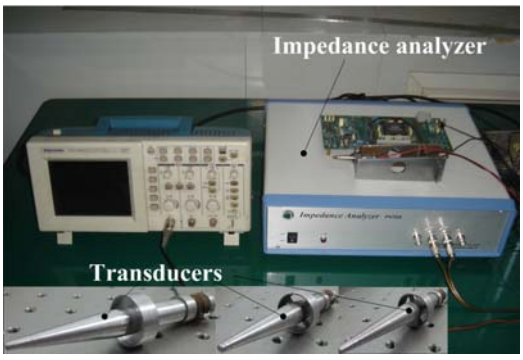

Fig. 14. Experimental setup for the impedance tests.

TABLE V
VIBRATION FREQUENCIES OF THE TRANSDUCERS BY IMPEDANCE TESTS

Flange type	Ring	Prismatic beam	Circular notched hinge
Frequency (kHz)	126.6	125.80	125.52

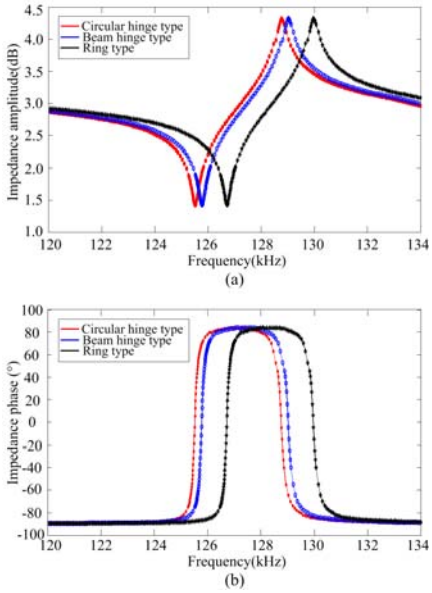

Fig. 15. Impedances of the transducers.

VI. Conclusion

The design, dynamic analysis and experimental test of high frequency piezoelectric ultrasonic transducers with flexure decoupling flanges for thermosonic bonding have been reported in this paper. By use of electromechanical equivalent method, the initial geometric dimensions of the transducers have been calculated. Then the transducers have been optimized using 3D FEM, and the geometric dimensions of the transducers have been determined. Flexure decoupling flanges have been presented and the decoupling principle of the flanges has been presented through stiffness comparison of the three types of decoupling flanges based on compliance matrix method and FEA. The dynamic characteristics of the transducers and their components have been analyzed through FEA. The longitudinal vibration frequencies of the piezoelectric converter and the concentrator without flange are 125.2 kHz and 125.6 kHz, respectively. The displacement amplitude nodes have been figured out, and the transducers composed of the piezoelectric converter and concentrators were modeled and analyzed. The results show that the longitudinal vibration frequencies of the transducers with ring, prismatic beam and circular notched hinge based decoupling flanges are 126.12 kHz, 125.70 kHz and 125.58 kHz, respectively, and there are no other vibration modes parasitizing closely to the longitudinal vibration mode. The ultrasonic vibration was generated by the piezoelectric ceramics, then transmitted to the front slab and amplified by the concentrators. The tip displacement amplitude of the transducers can reach up to 1.5 μm, 1.7 μm and 1.8 μm, respectively when applying the voltage U=10sinωt to the ceramics. The transducers have been manufactured and experimental impedance tests were carried out using an impedance analyzer. The experimental results match well with the FEA. The results show that the longitudinal vibration frequencies of the transducers are 126.60 kHz, 125.80 kHz and 125.52 kHz, respectively. The decoupling flange with circular notched hinges exhibits the best decoupling effect among the three types of flanges. The design method not only can overcome the difficulty in establishing the exact mathematical model of transducer with irregular shapes only by analytical methods, but also can solve the difficulty in determining the initial dimensions of the transducers solely depending on FEM. Through FEM, the transducer is optimized, and thus avoiding the repeated modeling, modifications and modal coupling. The 3D structural characteristics and optimization design were both considered during the design process, so the design accuracy and efficiency have been improved.

References

[1] H. Tang and Y.M. Li, "Development and active disturbance rejection control of a compliant micro/nano-positioning piezo-stage with dua-mode," *IEEE Transactions on Industrial Electronics*, vol.61, no. 3, pp.1475-1492, 2014.

[2] Q. Xu, "Design and development of a compact flexure-based XY precision positioning system with centimeter range," *IEEE Transactions on Industrial Electronics*, vol. 61, no. 2, pp. 893-903, 2014.

[3] L. Zhang, J.Y. Dong, and P.H. Cohen, "Material-insensitive feature depth control and machining force reduction by ultrasonic vibration in AFM-based nanomachining," *IEEE Transactions on Nanotechnology,* vol. 12, no. 5, pp. 743-750, Sep. 2013

[4] H.C. Liaw and B. Shirinzadeh, "Robust adaptive constrained motion tracking control of piezo-actuated flexure-based mechanisms for micro/nano manipulation," *IEEE Transactions on Industrial Electronics*, vol. 58, no. 4, pp. 1406–1415, Apr. 2011

[5] F.L Wang, J.H. Li, S.H. Liu, and L. Han, " Heavy aluminum wire wedge bonding strength prediction using a transducer driven current signal and an artificial neural network," *IEEE Transactions on Semiconductor Manufacturing*, vol. 27, no. 2, pp. 232-237, 2014.

[6] C.P. Chong, H.L. Li, H.L.W. Chan, and P.C.K. Liu, "Study of 1-3 composite transducer for ultrasonic wirebonding application," *Ceramics International*, vol.30, pp. 1141-1146, 2004.

[7] F.J. Wang, X.Y. Zhao, D.W. Zhang, and Y.M. Wu, "Development of novel ultrasonic transducers for microelectronics packaging," *Journal of Materials Processing Technology*, vol. 209, no. 3, pp. 1291-1301, 2009.

[8] S.W. OR, "High frequency transducer for ultrasonic bonding," Doctor Degree Dissertation, The Hong Kong Polytechnic University，Hong Kong, 2001.

[9] A.J. Fleming, and S.O.R. Moheimani, "Inertial vibration control using a shunted electromagnetic transducer," *IEEE/ASME Transactions on Mechatronics*, vol. 11, no. 1, pp. 84-92, 2006.

[10] H.J. Zhang, F.J. Wang, X.Y. Zhao, D.W. Zhang, and Y.L. Tian, "Electrical matching of low power piezoelectric ultrasonic transducers for microelectronic bonding," *Sensors and Actuators A: Physical*, vol. A199, pp. 241-249, 2013.

[11] G.Y. Gu, L.M. Zhu, C.Y. Su, and H. Ding, "Motion control of piezoelectric positioning stages: modeling, controller design and experimental evaluation," *IEEE/ASME Trans. Mechatronics*, vol. 18, no. 5, pp. 1459–1471, Oct. 2013.

[12] Y.X. Liu, W.S. Chen, J.K. Liu, and X.H.Yang, "A high-power linear ultrasonic motor using bending vibration transducer", *IEEE Transactions on Industrial Electronics*, vol. 60, no. 11, pp. 5160-5166, Nov. 2013.

[13] H-L Cheng, C-A Cheng, C-C Fang, and H-C Yen, "Single-switch high-power-factor inverter driving piezoelectric ceramic transducer for ultrasonic cleaner", *IEEE Transactions on Industrial Electronics*, vol. 58, no. 7, pp. 2898-2905, July 2011.

[14] Y.X. Liu, W.S. Chen, J.K. Liu, and X.H.Yang, "A rotary piezoelectric actuator using the third and fourth bending vibration modes", *IEEE*

Transactions on Industrial Electronics, vol. 61, no. 8, pp. 4366-4373, Aug. 2014.

[15] S. Narasimalu, and S.K. Balakrishnan, "Bonding apparatus comprising improved oscillation amplification device," *U.S. Patent*, US0084900AL, 2007.

[16] M. Sakakura, "Ultrasonic transducer for a bonding apparatus and method for manufacture the same," *U.S. Patent*, US6578753B1, 2003.

[17] L.M. Zhang, Y.J. Liu, and L.N. Sun, "Research on a new composite ultrasonic energy transmission system with the serial structure," *In Proceedings of the 2007 IEEE International Conference on Mechatronics and Automation*, Harbin, China, Aug. 2007, pp. 1639-1644.

[18] J . Tsujino, H. Yoshihara, and T. Sano, "High-frequency ultrasonic wire bonding systems," *Ultrasonics*, vol.38, no. 1, pp. 77-80, 2000.

[19] S. Sherrit, H.D. Wiederick, B.K. Mukherjee, M. Sayer, An accurate equivalent circuit for the unloaded piezoelectric vibrator in the thickness mode, *Journal of Physics D: Applied Physics* vol. 30, 2354–2363, 1997.

[20] M.V. Arx, "Novel ultrasonic transducer design for fine-pitch wire bonding," *In Proceedings of IEEE/CPMT International Electronic Manufacturing Technology Symposium*, NA, USA, 2003, pp. 49-53.

[21] S.-H. Wang, and M.-C. Tsai, "Dynamic modeling of thickness-mode piezoelectric transducer using the block diagram approach," *Ultrasonics*, vol. 51, no. 5, pp. 617-624, Jul. 2011

[22] S.Y. Lin, L. Xu and W.X. Hu, "A new type of high power composite ultrasonic transducer," *Journal of Sound and Vibration*, vol. 330, no. 7, pp. 1419-1431, Mar. 2011

[23] L. Parrini, "New techniques for the design of advanced ultrasonic transducers for wire bonding," *IEEE Transaction on Electronics Packaging Manufacturing*, vol. 37, no. 1, pp. 37-45, 2003.

[24] S.W. Or, H.L.W. Chang, and P.C.K. Liu, "Piezocomposite ultrasonic transducer for high-frequency wire-bonding of microelectronics devices," *Sensors and Actuators A: Physical*, vol. A133, pp. 195-199, 2007.

[25] S.W. Or, H.L.W Chan, and V.C. Lo, "Dynamics of an ultrasonic transducer used for wire bonding," *IEEE Transaction on Ultrasonics, Ferroelectrics, and Frequency Control*, vol. 45, no. 6, pp. 1453-1460, 1998.

[26] L. Parrini, "Design of advanced ultrasonic transducers for welding devices," *IEEE Transactions on Ultrasonics, Ferroelectrics and Frequency Control*, vol. 48, no. 6, pp. 1632-1639, Nov. 2001.

[27] Z.L. Long, Y.X. Wu, and L. Han, "Dynamics of ultrasonic transducer system for thermosonic flip chip bonding," *IEEE Transaction on Components and Packaging Technologies*, vol. 32, no. 2, pp. 261-267, 2009.

[28] L.-C. Cheng, Y.-C. Kang, and C.-L. Chen, "A resonance-frequency-tracing method for a current-fed piezoelectric transducer", *IEEE Transactions on Industrial Electronics*, vol. 61, no. 11, pp. 6031-6040, Nov. 2014.

[29] S.Y. Lin, "The Principle and design of ultrasonic transducers", Science Press, Jun. 2004.